Materials Today Bio 32 (2025) 101811

Contents lists available at ScienceDirect

Materials Today Bio

journal homepage: www.journals.elsevier.com/materials-today-bio

Zwitterion nanocomposite hydrogels with bioactivity and anti-adhesion properties for rapid prevention of postoperative and recurrent adhesion

Weihan Zhu [a,1], Jintao Fang [a,1], Wenjun Xu [a,1], Dian Yu [a], Jintao Shi [a], Qing Xia [a,b,*], Jinwei Wang [c], Xiaohui Chen [c], Haorui Zha [a], Shengyu Li [a,d,e,**], Wei Zhang [a,d,e,***]

[a] The Second Affiliated Hospital and Second Clinical Medical School, Zhejiang Chinese Medical University, Hangzhou, 310000, PR China
[b] Zhejiang Provincial People's Hospital, Hangzhou, 310000, PR China
[c] Medical Research Center, Academy of Chinese Medical Sciences, Zhejiang Chinese Medical University, Hangzhou, 310000, PR China
[d] Key Laboratory of Pathogenesis Research of "Inflammatory-Cancer Transformation" in Intestinal Diseases, Hangzhou, 310000, PR China
[e] Zhejiang Engineering Research Center of Intelligent Equipment of Chronic Chinese and Western Medicine, Hangzhou, 310000, PR China

ARTICLE INFO

Keywords:
Nanosilicate
Zwitterionic hydrogels
Postoperative adhesions
Nonfouling performances

ABSTRACT

Postoperative adhesions (PAs) are a common complication after intraperitoneal surgery. Hydrogels are a physical barrier that prevents peritoneal adhesions, but their efficacy is still controversial. In this study, Laponites, a layered two-dimensional nanoscale, is incorporated into zwitterionic hydrogel (pSBLA) to enhanced biocompatibility and bioactivity to develop a nanocomposite for rapid prevention of postoperative and recurrent adhesion. The anisotropic distribution of charges in laponites results in strong hydrogen bonding and electrostatic repulsion in aqueous solutions and enables hydrogen bonding between amphiphilic ions, thereby enhancing the mechanical properties of hydrogels. The pSBLA hydrogels also possess a series of characters for an ideal anti-adhesion material, including resistance to adhesion against fibrinogen, proteins as well as cells. The mechanism underlying the extraordinary hydration of pSBLA is elucidated in this study using molecular dynamic simulations. In addition, pSBLA hydrogel is shown to represent a major advancement in anti-adhesion efficacy by completely and reliably preventing postoperative and recurrent adhesions after adhesiolysis in rat models. Furthermore, mechanistic explorations revealed that pSBLA hydrogel inhibits inflammatory responses and resists fibrosis by regulating the transforming growth factor-β/Smad signal pathway. Therefore, the pSBLA hydrogel has considerable potential for preventing post-operative adhesions in clinical settings.

1. Introduction

Postoperative adhesions (PAs) are an inevitable health issue in abdominal and pelvic surgeries, which results from systemic dysregulation involving clotting, inflammation, fibrinolysis, and other factors [1]. The incidence of peritoneal adhesions in patients undergoing abdominal surgery can be as high as 90 % [2,3]. This common postoperative complication can excessively bind organs and tissues, leading to severe clinical symptoms, including intestinal obstruction, abdominal pain, dyspepsia, and can even result in death owing to improper treatment [3]. A high probability of peritoneal adhesions within the first year after gastrointestinal surgery has been reported, which may necessitate further surgery to remove the adhesions [4]. Currently, the approaches for eliminating the formation of adhesions primarily include pharmaceutical treatment and the use of biological barrier materials after the first surgery. However, drug-based strategies are typically ineffective and may result in undesirable side effects. For instance, systemic administration of fibrinolytic drugs can lead to bleeding complications [5]. In contrast, biological barrier materials directly separate damaged tissues at the surgical site from surrounding normal organs, which have been successfully used to treat any adhesion [6]. Interceed and Sepraflm have received approval from Food and Drug Administration for clinical use. However, their application process is inconvenient; and requires meticulous hemostasis and effective suturing on the injured

* Corresponding author. Zhejiang Provincial People's Hospital, Hangzhou, 310000, PR China.
** Corresponding author. The Second Affiliated Hospital and Second Clinical Medical School, Zhejiang Chinese Medical University, Hangzhou, 310000, PR China.
*** Corresponding author. The Second Affiliated Hospital and Second Clinical Medical School, Zhejiang Chinese Medical University, Hangzhou, 310000, PR China.
E-mail addresses: xiaqing19821031@126.com (Q. Xia), 18768393817@163.com (S. Li), zhangweils1968@163.com (W. Zhang).
[1] These authors contributed equally.

https://doi.org/10.1016/j.mtbio.2025.101811
Received 10 December 2024; Received in revised form 11 April 2025; Accepted 26 April 2025
Available online 28 April 2025

tissue surface; otherwise, forming a conformal barrier on an irregular surface becomes difficult [7–9]. In comparison, hydrogel-based physical barriers are widely studied due to their excellent biocompatibility and mechanical properties, and complete wound coverage [10]. However, a lack of bioactivity is a drawback, and their usage other limitations [11]. For instance, hyaluronic acid (HA) or its derivative hydrogel has a limited range of applications and cannot completely prevent adhesion and need to be used in combination with drugs [12–14]. Therefore, existing physical barrier technologies under-performance and can only alleviate or reduce adhesions to some extent. Therefore, designing an effective barrier for decreasing the incidence of PAs is critical.

Zwitterionic materials have excellent biocompatibility and are effective in preventing nonspecific protein adsorption, and have gained widespread attention in recent years [15–17]. They consist of equal positive and negative charges, which render them electrically neutral. Strong surface hydration is found to act as a barrier against biomolecules, preventing them from being adsorbed on submerged surfaces and is generally regarded as a crucial factor in providing a physical barrier against protein and cell adsorption [18–20]. Jiang prepared nonfouling zwitterionic materials, and demonstrated their nonfouling properties under highly challenging conditions [21]. A zwitterionic hydrogel prepared by crosslinking carboxybetaine acrylamide and N, N′-bis(acryloyl) cystamine, has been used to prevent postoperative abdominal adhesion [22]. However, the weak mechanical properties of zwitterionic hydrogels limit their application in PAs. The optimization of mechanical properties of hydrogels can improve their stability and durability in vivo, so as to better prevent postoperative adhesion [23]. In addition, several zwitterionic biodegradable hydrogels are reported to increase biosafety and related risks [24,25]. Thus, a favorable hydrogel barrier should completely cover the surface of damaged tissue, possess excellent mechanical properties to withstand external forces during surgery, resist protein adsorption, reduce fibrin deposition, and prevent fibroblast adhesion. Moreover, the materials should have excellent biocompatibility to avoid triggering local inflammatory responses or hemolysis [26,27].

Laponite, a layered two-dimensional nanoscale, it has been extensively studied in the field of regenerative medicine to improve the structure, properties and properties of various biological materials

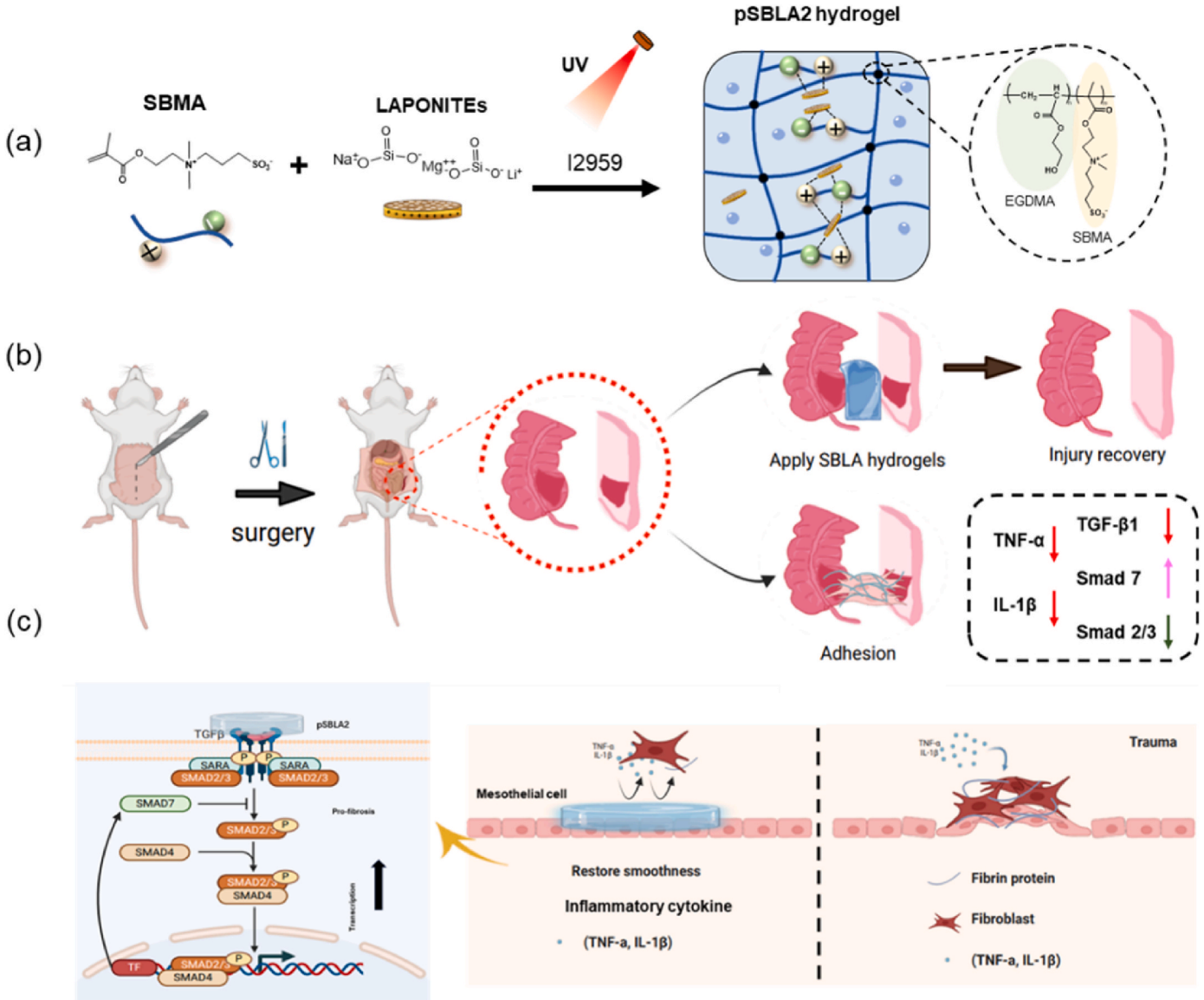

Scheme 1. (a) Schematic illustration of the formation of the pSBLA hydrogel. (b) Cecum-abdominal wall adhesion model establishment and different effects with or without the treatment of pSBLA2 hydrogel. (c) Schematic depicting the process and mechanism of the hydrogel for inhibiting postoperative abdominal adhesion. (Created with BioRender.com).

(Fig. S1, supporting information) [28]. These particles form delaminated dispersions in water which self-organize via hydrogen bonding and electrostatic interactions forming an open, macro-porous and reversible (thixotropic) gel network [29]. Additionally, a substantial body of literature has been generated on laponite as a model system for drug delivery system that demonstrates the ability to localize and sustain the activity of bioactive substances over time, leading to improved safety and efficacy [30,31]. Despite intriguing data suggesting the inherent osteogenic bioactivity of laponites, no studies have yet successfully applied clay colloidal gels as a strategy to improve the mechanical properties of zwitterionic hydrogels. Compared with double-network hydrogels, asymmetric-structure hydrogels and electrospinning hydrogels, the preparation processes of these hydrogels are complex and involve special synthesis methods [32–34]. We supposed that the anisotropic distribution of charges in laponites results in strong electrostatic repulsion in aqueous solutions, facilitating electrostatic interactions and hydrogen bonding between amphiphilic ions and thereby enhancing the mechanical properties of hydrogels to withstand external forces during surgery. More importantly, this is the first study that has incorporated laponite into 3-[[2-(methacryloyloxy)ethyl](dimethyl)-ammonio]-1-propanesulfonate monomers (SBMA) to enhance the mechanical properties and bioactivity of hydrogels and to prevent postoperative adhesion.

In this study, we aimed to prepare nanocomposite amphiphilic hydrogels (pSBLA) through ultraviolet polymerization in an aqueous solution of laponite and SBMA (Scheme 1a). This study provides new insights into how laponite incorporation in a hydrogel microenvironment—via a simple mix and crosslink approach—affects cell proliferation and culture. The pSBLA hydrogel was assessed for mechanical strength to maintain its integrity when implanted and to completely cover irregular wounds its nonfouling capabilities, biocompatibility during prolonged in vivo implantation, and its inhibitory potential on the formation of postoperative peritoneal adhesion through the transforming growth factor beta (TGF-β)/suppressor of mothers against decapentaplegic (Smad) signaling pathway (Scheme 1). The pSBLA hydrogel is an ideal candidate for the prevention of postoperative tissue adhesion.

2. Experimental section

2.1. Materials

3-[2-(methacryloyloxy)ethyl](dimethyl)-ammonio]-1-propanesulfonate (SBMA, 98 %), Photoinitiator Irgacure 2959 (I2959), ethylene glycol dimethacrylate (EGDMA), N, N, N′, N′-tetramethylethylenediamine (TEMED, 98 %) were purchased from Sigma-Aldrich Chemical Co., Ltd. (China). Laponites was provided by Macklin. Live/Dead viability and cytotoxicity kit were all pursued from Sigma-Aldrich (United States). IL-1β, TNF-α and TGF-β1 ELISA kits were all pursued from Kndbio Biotechnology Co., Ltd. (China). Mouse anti-rat Smad 2/3 antibodies were obtained from Abcam. Rabbit anti-rat Smad7 antibodies were obtained from Sanying Biotechnology. Alexa Fluor® 488-conjugated goat anti-mouse IgG and anti-rabbit IgG were obtained from ThermoFisher. Hyaluronic acid (HA) gel dressing was obtained from Zhejiang Jingjia Medical Technology Co., Ltd. (China). Deionized water (18.2 MΩ cm) was prepared before use.

2.2. Preparation of pSBLA hydrogels

The pSBLA hydrogels were prepared using the following method. The monomers SBMA (4M) were first fully dissolve in 0.5 %, 1 % and 2 % Laponites solution, respectively. The crosslinker EGDMA (1 % versus monomer w/w), I2959 initiator (1 % versus monomer w/w) and TEMED (0.1 %, v/v) were added and complete dissolved to the above solutions at room temperature. After thorough mixing and degassing, the solution was transferred into two glass slides with a 1 mm poly (tetrafluoroethylene) spacer, and the hydrogel was prepared with 365 nm UV light for 60 min. Finally, the hydrogels were followed by equilibration in sterile water for 3 days. To facilitate further discussion, we designated the prepared hydrogels as pSBLA0.5, pSBLA1, pSBLA2, respectively. As the control, the pSBMA hydrogel was prepared by dissolving SBMA in water with the same method.

2.3. Characterization

The hydrogels were freeze-dried and sprayed with gold. The surface morphology and element distribution of hydrogels was examined by a field emission scanning electron microscopy (SU8010, Hitachi Limited, Japan). The molecular structure of the hydrogels was confirmed by a Fourier transform infrared (FTIR) spectrometer (Thermo Fisher Nicolet iS50, USA). X-ray photoelectron spectroscopy (XPS) was taken to confirm the structure of samples by a Kα instrument (Thermo Scientific K-Alpha) with a 1 eV of energy step and 100 eV pass energy. Thermogravimetric analysis (TGA, TA-Q600) was carried out to detect the thermal properties of the samples.

2.4. Platelet adhesion

Anticoagulant whole blood was first separated (800 rpm, 15 min) to obtain the platelet-rich plasma (PRP). Then hydrogels were placed into ep-tube incubated with 1 mL of PRP at 37 °C for 1h. After that, the hydrogels were washed with PBS to remove non-adsorbed platelet. Then, the hydrogels were incubated with 1 mL of PBS at 37 °C for 1h to release the remaining platelet. Finally, the optical density (OD) of the remaining plasma was measured at 450 nm.

2.5. Protein adsorption test

Bovine serum albumin (BSA) and fibrinogen were selected as the model protein to assess the protein adsorption of the hydrogel. Firstly, the swelling equilibrium hydrogels were immersed in 2 mL of BSA solution (2 mg/mL). After incubating for 6h at 37 °C, the hydrogels were washed three times with PBS to remove non-adsorbed proteins. Finally, according to the instructions, the BCA protein quantification assay kit was used to determine the protein content in the eluate, and the experiments were repeated in triplicate. Besides, fibrinogen adsorption test was evaluated by fibrinogen kit as the instructions of manufacturer and performed at 492 nm, and the experiments were repeated in triplicate.

2.6. Cell adhesion test

NIH/3T3 cells were selected to evaluate the anti-cell adhesion properties of the hydrogels. SBLA hydrogel disks were first soaked in 70 % ethanol for 2 h for sterilization and soaked in sterilized PBS until equilibrium. Subsequently, cells were respectively seeded onto hydrogel disks at a concentration of 10^5 cells/mL into 24-well plates and incubated for 24h at 37 °C. Then, cells on the hydrogels were stained by Calcein-AM and photographed on a fluorescence microscope (ECLIPSE TI-S, Nikon, Japan).

2.7. Establishment of abdominal sidewall-cecal injury model

The male SD rats (180 ± 20 g) were purchased from Zhejiang Chinese Medicine University Laboratory Animal Research Center. The protocols used for the animal experiments procedure was passed the "Guiding Principles in the Care and Use of Animals, revised in 2017" (China), and the study was approved by Institutional Animal Care and Use Committee of Zhejiang Chinese Medicine University (IACUC-20240708-02).

The rats were anesthetized by injection of atropine and Zoletil 50, and then secured on the experimental operating table. After the

abdomen hair was shaved, a 5 cm incision was carried out along the centerline of the lower abdomen skin. The right abdominal wall of the rat was clamped with hemostatic forceps, and the cecum was gently picked out and abraded using sterile gauze until a petechial hemorrhage appeared on the surface of the cecum. A tweezers was used to create a 2 cm by 2 cm peritoneal defect on the corresponding side of the abdominal wall. Later, the cecum injury was attached closely to the corresponding abdominal wall defect by fixing with 3-0 sutures [11,27,35].The model group was washed with 1 mL of physiological saline. For the HA and pSBLA2 hydrogel groups, the wounds were covered with HA and pSBLA2 hydrogels, respectively. The rats in the control group were without any treatments. Finally, the abdominal muscle layer and skin layer was closed. All experimental procedures were performed under sterile conditions. After 7 and 14, 4 rats from each group were sacrificed to evaluate the anti-adhesion efficiency of the hydrogels.

2.8. Establishment of a repeat adhesion model after adhesiolysis

A recurrent adhesion model after adhesiolysis was established as described above. After the establishment of the abdominal adhesion model, the abdominal cavity was opened again for repeated adhesion model on day 7. And the adhesions between the cecum and abdominal wall were separated by blunt dissection. The separated cecum and abdominal wall were wiped with sterile gauze, until bleeding wound appeared again on the surface of the cecum. Subsequently, pSBLA2 hydrogel, medical HA hydrogel and model group were treated similarly to the method of the previous model. 7 days after adhesiolysis, the rats were sacrificed to evaluate the anti-adhesion efficiency.

2.9. Statistical analysis

Statistical analysis performed using Origin 2022 software and GraphPad Prism software. All data were reported as means ± standard deviations. Differences among groups were analyzed with one way analysis of variance (ANOVA). A value of $p < 0.05$ was considered significant.

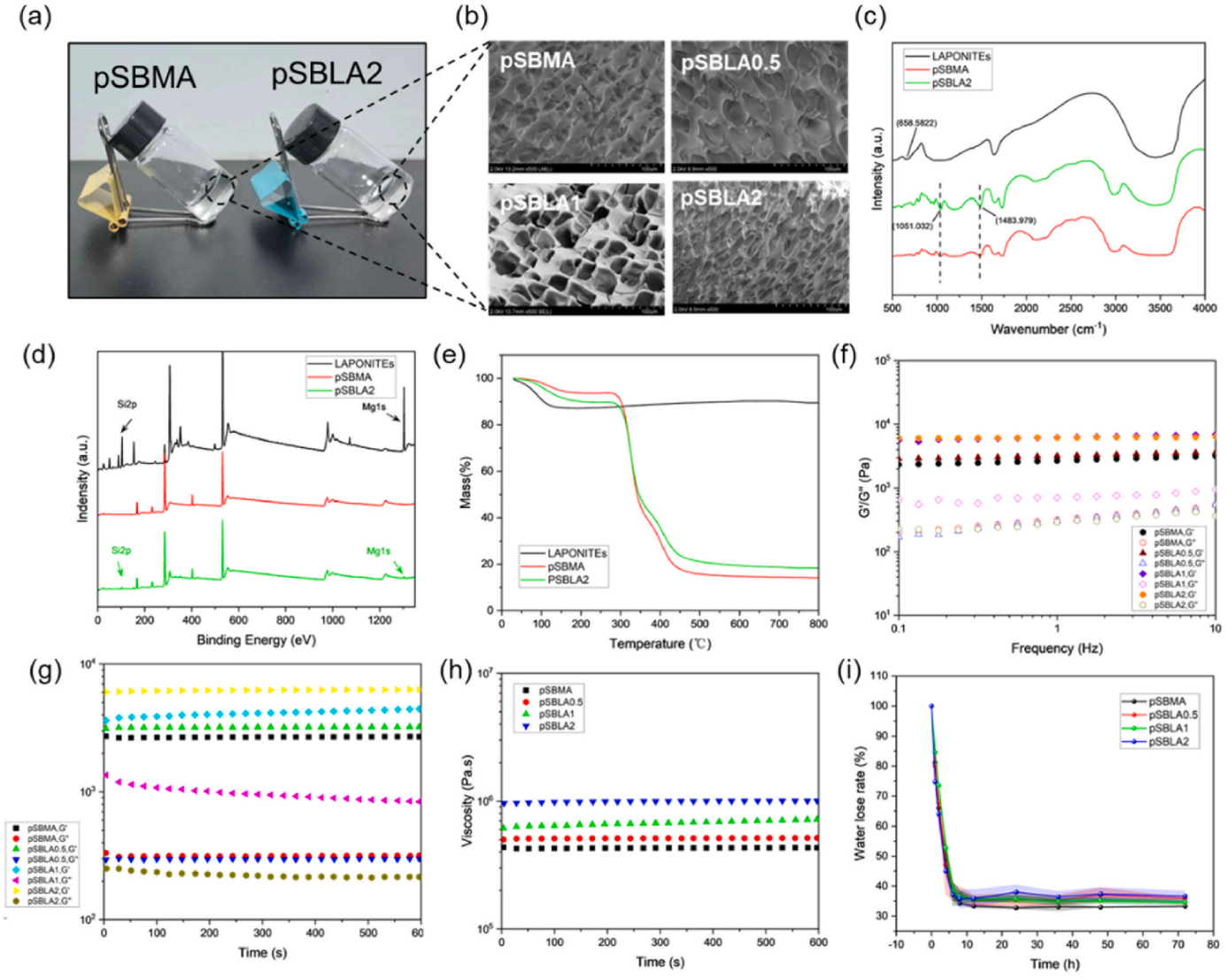

Fig. 1. Characterization of pSBLA hydrogels. (a) The optical photograph of pSBMA and pSBLA2 hydrogel in synthesis vial. (b) The interior structure of the dry materials. Scale bar = 50 μm. (c) FT-IR spectra and (d) XPS diagram of pSBLA2, pSBMA, Laponites. (e) TGA curve of Laponties, pSBMA, and pSBLA2 hydrogels. (f) The rheological characterization of hydrogels in frequency-sweep (0.1–10 Hz, strain of 1 %), (g) in time-sweep curves (10 min, 1 Hz, strain of 1 %, 37 °C), and (h) viscosity curves with a low strain at 1 %. (i) The water lose rate of pSBMA, pSBLA0.5, pSBLA1, and pSBLA2.

3. Results and discussion

3.1. Preparation and characterizations of pSBLA hydrogels

We synthesized a new class of antifouling polymer hydrogels, pSBLA, by photoinitiation of laponites (synthetic hectorite-type clay) and SBMA (Scheme 1a). Laponite consists of discs (1 nm thick and 25 nm in diameter) that are made up from tetra-octa-tetra layers. Net negative charges can occur on the surface through isomorphous substitution by substituting Mg^{2+} with Li^{+} in the octahedral sheet [36]. In SBLA solution, hydrophilic SBMA enhances the zeta potential of laponite, through electrostatic interactions (Fig. S2, Supporting Information) [37,38]. We propose that pSBLA hydrogels have sufficient mechanical strength to adapt to the integrity when implanted owing to enhanced hydrogen bonding [39]. Upon binding with water, the zwitterionic segments of pSBLA hydrogels form a strong surface hydration that resists protein adsorption and cell attachment. Compared to other conventional physical hydrogels, the pSBLA hydrogel demonstrates excellent resistance to protein adsorption, minimizing foreign body reactions to a maximum extent.

A series of amphiphilic ion-water hydrogels with varying laponite concentrations were synthesized (pSBLAn, where n denotes the laponite content). The pSBMA and pSBLA2 hydrogels are transparent materials that will not fall if placed on their sides (Fig. 1a). The lyophilized pSBMA, pSBLA0.5, pSBLA1, and pSBLA2 hydrogels exhibited a three-dimensional network structure (Fig. 1b) indicating that laponite did not alter the original morphological characteristics of the hydrogels. The Fourier-transform infrared spectra (FT-IR) of the laponite, pSBMA, and pSBLA2 hydrogels are shown in Fig. 1c. The characteristic absorption peaks at 1051 and 1483 cm^{-1} for pSBMA and pSBLA2 were mainly attributed to the symmetric and asymmetric stretching vibrations of $-SO_3H$ groups, respectively. The pSBLA2 hydrogel exhibited Si-O-Si stretching bands at 650 cm^{-1}, which had a weak shift compared to that of bare laponite (658 cm^{-1}). The C=O stretching band of the pSBMA hydrogel at 1655 cm^{-1} showed a shift comparable to that of pSBLA2 (1660 cm^{-1}), which confirmed the crosslinking between laponites and polymer chains through hydrogen bonding. Fig. 1d shows the X-ray photoelectron spectra of the laponite, pSBMA, and pSBLA2 hydrogels. Owing to the presence of laponites, pSBLA2 had additional peaks (1304.1 and 103.1eV) at Mg1s and Si2p, respectively. The binding energy range for C1s components of pSBMA and pSBLA2 is shown Fig. S3. There are C=O (286.3 eV), C-C (284.7 eV), C=C (288.5 eV) bonds for pSBMA and pSBLA2, showing that laponites reacts with pSBMA hydrogels mainly through hydrogen bonding and electrostatic interactions. The thermogravimetric analysis (TGA) showed that all the hydrogels exhibited two stages of decomposition, whereas the laponites showed only one (Fig. 1e). The first stage of degradation was marked by a loss of crystalline water from the material. Among them, the maximum degradation temperature for pSBMA was 429.6 °C with a mass loss of 74.4 %, which was attributed to the decomposition of pSBMA macromolecular chains. The maximum degradation temperature for pSBLA2 was 440.3 °C with a mass loss of 81.9 % that was 10.7 °C higher than that of pSBMA indicating increased thermal stability. In addition, both pSBMA and pSBLA2 contained C, N, S, and O in the energy dispersive spectrum analysis (Fig. S4, Supporting Information). The contents of Mg in pSBLA2 were 4.98 % which was mainly originated from laponite. Moreover, Mg element was uniformly distributed in PSBLA2 hydrogel, which also proved that laponite is uniformly distributed in hydrogels. Those results indicated that pSBLA2 successfully grafted laponites.

3.2. Mechanical behavior of the pSBLA hydrogel

The rheological behavior of the hydrogels (pSBMA, pSBLA0.5, pSBLA1 and pSBLA2) was investigated using a rheometer to evaluate the effect of laponite on the mechanical properties of the hydrogels (Fig. 1f-h). The frequency sweep results showed that the G′ and G″ values for all hydrogels increased with an increase in frequency within the test frequency range (0.1–10 Hz). At low frequencies, G″ was higher than G′, indicating that all hydrogels behaved as a solid. As the laponite concentration increased, the G′ value increased from 2689 Pa (pSBMA) to 6257 Pa (pSBLA2). Conversely, with a further increase in frequency, the solid structure of the hydrogel gradually deteriorated (G'<G″). Furthermore, all hydrogels exhibited stable solid-like behavior because the G″ values were consistently higher than their respective G' at 1 Hz and 1 % strain (Fig. 1g). As the laponite concentration increased, the pSBLA2 hydrogels adopted sticky behavior (Fig. 1h). In addition, tensile tests were performed on the hydrogels. With an increase in the laponites concentration from 0 % to 2 %, the tensile stress of the pSBMA hydrogels gradually increased from 14.41 kPa to 51.01 kPa (Figs. S5 and S6, Supporting Information). Overall, the concentration of laponite possibly played a decisive role in the mechanical strength of pSBMA hydrogels. Based on the unique layered structure and negative surface charge, it interacted with the $(CH_3)_2\bar{N}^{+}$ and $-S\bar{O}_3$ of SBMA through hydrogen bonding and possible electrostatic forces, enhancing the mechanical properties of the hydrogel. Moreover, the rate of water loss of the hydrogels (Fig. 1i) suggested that laponite concentration did not alter the pSBMA hydrogel network. As shown in Fig. S7, the prepared hydrogels showed excellent swelling ability in PBS, with swelling in PBS attributed to zwitterionic segments.

3.3. In vitro biocompatibility of pSBLA hydrogels

The optical images of samples confirmed that all hydrogel-treated groups displayed clear supernatants with intact red blood cells (Fig. 2a). A quantitative analysis indicated that hemolysis induced by the hydrogels was ≤3 %, indicating satisfactory blood compatibility of pSBLA hydrogels (Fig. 2b).

To evaluate potential cytotoxicity, the gel extract was tested on NIH/3T3 cells and using a Cell Counting Kit-8 (CCK-8) assay. Cells were viable after 1 and 3d of incubation with all hydrogels, with cells surviving in the presence of all samples (green), indicating considerable cytocompatibility (Fig. 2c). In addition, the results of the CCK-8 assay showed that cell viability was ≥95 % in all hydrogel groups, indicating minimal cytotoxicity (Fig. 2d and e). With the extension of culture time, cell viability after co-culturing with the pSBLA2 hydrogel was significantly higher than that with other groups.

We further investigated the impact of the pSBLA2 hydrogels on cell biological activity by carrying out the wound scratch assay *in vitro*. The pSBLA2 hydrogels exhibited enhanced cell migration with narrower cell gaps compared to the control group at both 12 and 24 h after the treatments (Fig. 2f-h). These studies indicate the cytocompatibility of laponite encapsulation for cell proliferation and migration. As the chemical composition of Laponite is similar to bioactive glasses, which are composed of SiO_2, CaO and P_2O_5, the bioactivity of Laponites can be expected. We speculated that the considerable effects of pSBLA2 on cell activity and cell migration might be attributed to the laponite released from hydrogels [40,41].

3.4. In vitro fouling tests of pSBLA2 hydrogels

Protein adsorption fibroblast adhesion and proliferation are crucial factors in peritoneal adhesion formation [1]. Zwitterionic-SBMA-based hydrogels prevent nonspecific protein adhesion owing to the dense hydration layer of positive and negative charges on the surface [42]. Therefore, the pSBLA hydrogel may possess excellent nonfouling properties due to the zwitterionic-SBMA structure. Fibrinogen also plays a key role in peritoneal adhesion formation, as it serves as a foundation for fibroblast adhesion and is involved in tissue repair and scar formation [43]. Therefore, we first polymerized pSBMA, pSBLA0.5, pSBLA1, and pSBLA2 hydrogels, which were then exposed to fibrinogen solution (10 mg/mL). After the exposure period, the amount of fibrinogen adhering to the hydrogel and tissue culture polystyrene (TCPS) was quantified

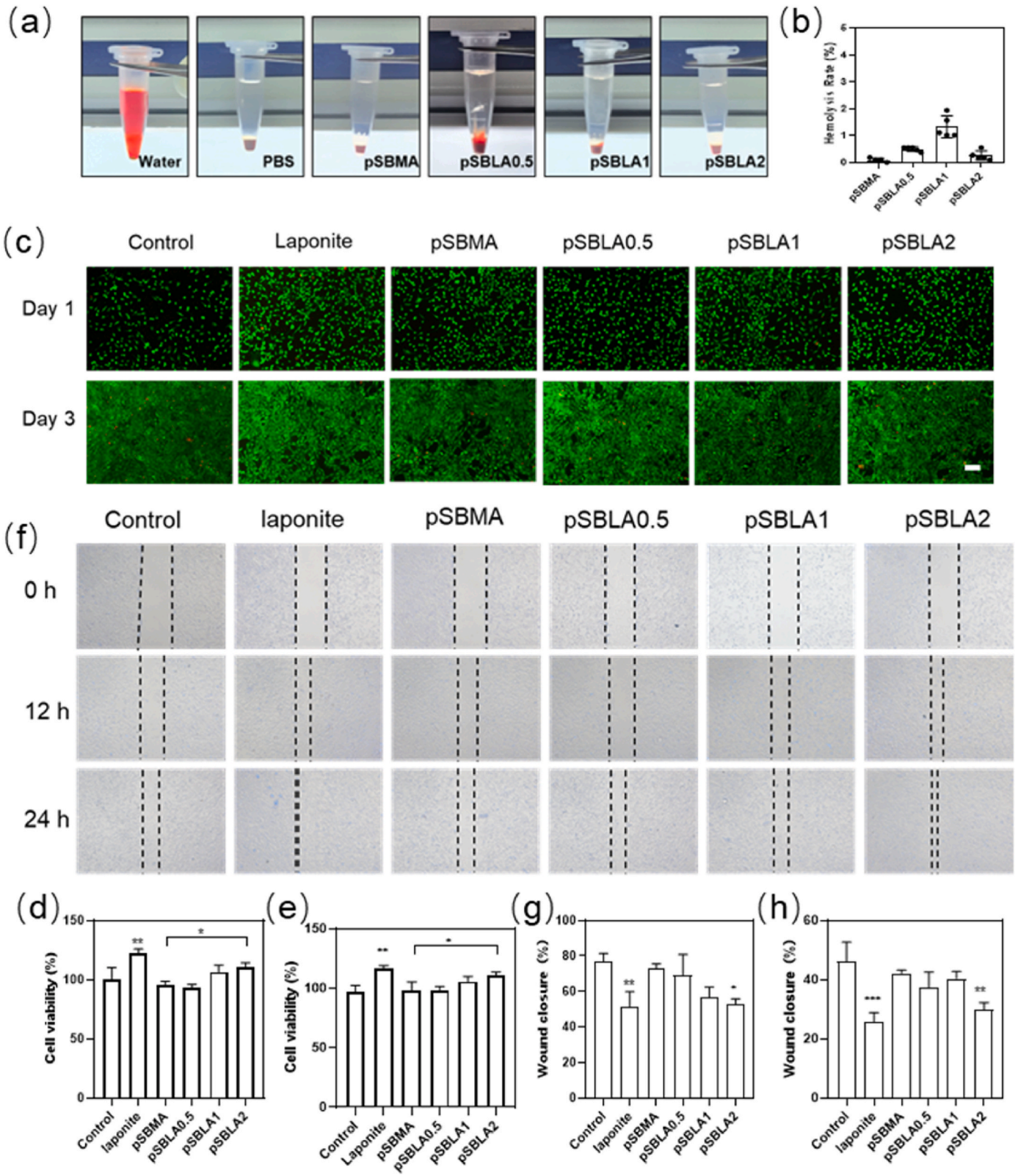

Fig. 2. The biocompatibility of pSBLA hydrogels *in vitro*. The images (a) and quantitative statistics (b) of blood incubated with hydrogels. (c) Live/dead cell viability assay. NIH/3T3 fibroblast cells were incubated with both the hydrogel extract for 24 h and 72 h. In the assay, live cells stain green and dead cells stain red, as viewed with a fluorescent microscope. Scale bar = 100 μm. CCK-8 assay for evaluation of cytotoxicity of different samples for 24 h (d) and 72 h (e). (Data presented as mean ± SD, n = 3, $^{**}p < 0.001$, compared with the control group). (f) In vitro scratch assay, scale bar = 100 μm. Quantified data of the migration rate (mobility ratio) after the treatments with the different samples for 12 h (g) and 24 h (h) (n = 3, $^{***}p < 0.001$, $^{**}p < 0.01$, and $^{*}p < 0.05$, compared with the control group). (For interpretation of the references to colour in this figure legend, the reader is referred to the Web version of this article.)

using enzyme-linked immunosorbent assay (ELISA) (Fig. 3a). The hydrogel disks exhibited exceptional nonfouling potential compared to that of TCPS. In addition, proteins promote adhesion formation. Herein, all hydrogels had a lower protein adsorption capacity than that of TCPS and the results with blood platelets were similar (Fig. 3b and c).

Cell adhesion is a major form of biological fouling; for instance, extensive secretion of collagen by fibroblasts causes the mature development of adhesions. The potential of pSBLA against cell adhesion was also investigated by seeding NIH/3T3 fibroblasts onto pSBLA hydrogel discs and analyzing the number of adherent cells in culture after 1 day (Fig. 3d). A large cluster of fibroblast cells was observed in TCPS, whereas the surface of pSBLA2 hydrogel discs remained clean, with few adherent fibroblast cells, indicating the exceptional nonfouling property of pSBLA2 hydrogel.

3.5. Molecular mechanism of nonfouling of SBMA

The pSBLA hydrogels exhibited excellent nonfouling properties, which may be attributed to the highly hydrophilic nature of zwitterionic SBMA monomers and their unique hydration characteristics. To confirm our hypothesis, we conducted molecular dynamics (MD) simulations to understand the underlying mechanism of nonfouling potential of the hydrogels. We performed MD simulations of a single SBMA molecule and a 10-residue pSBMA in an aqueous solution, with a three-residue polyethylene glycol oligomer (OEG) serving as control. Remarkably, there was an average of 2.5 hydrogen bonds from water, providing oxygen for SBMA; however, the OEG oxygen atoms accepted only one (Fig. 4a). In simulation, the life-time of hydrogen bond (τ_{HB}) between SBMA and water was longer than that between OEG and water (Fig. 4b), indicating that SBMA has a strong interaction with multiple water molecules. As shown in Fig. 4c, the radial distribution functions (RDFs) of water oxygen atoms respect to the heavy atoms of the O, N, and S atoms in the SBMA small molecule reveal a near-contiguous sphere of hydration centered on the sulfonic acid group, which was continuous (O_{SBMA}, N_{SBMA}, and S_{SBMA}, respectively). Fig. 4d showed a single frame from the SBMA monomer simulation, including the water molecules with O_{SBMA}-water oxygen (high opacity), N_{SBMA}-water oxygen, and S_{SBMA}-water oxygen distances less than the RDF peak value, respectively. Remarkably, the hydration shell was also observed in pSBMA (Fig. 4e), indicating that water was similarly ordered near the pSBMA headgroups. Taken together, the MD simulations suggest that pSBMA retains the superhydrophilicity observed for the SBMA small molecule, which can provide a strong surface hydration. Our study reveals that the interplay among hydrogen bonding, super-hydrophilic nature, and contiguous hydration shells is crucial to the fouling-resistant capabilities of zwitterionic hydrogels. As a result of the extension conjecture, it is possible that pSBLA hydrogels exhibit nonfouling properties because pSBLA2 hydrogel has super-hydrophilic SBMA fragments.

3.6. Evaluation of tissue adhesion prevention in vivo

To validate the efficacy of pSBLA hydrogel in preventing PA, we established a sidewall defect-cecum abrasion model in rats (Fig. 5a) [23, 44]. Rats received no treatment as negative a control (Model) or HA hydrogel (the leading commercial antiadhesive) as a positive control (HA). Further, the healthy rats served as the control group (Control). Throughout the animal experiments, no adverse reactions such as bleeding, infection, or unexpected death were observed. Their growth curves showed revealed that the rats gained appropriate weight, indicating they were in good health (Fig. S8, Supporting Information). On the 7th and 14th days post-surgery, the peritoneal cavities of the rats were reopened for observation, and the extent of PA among different

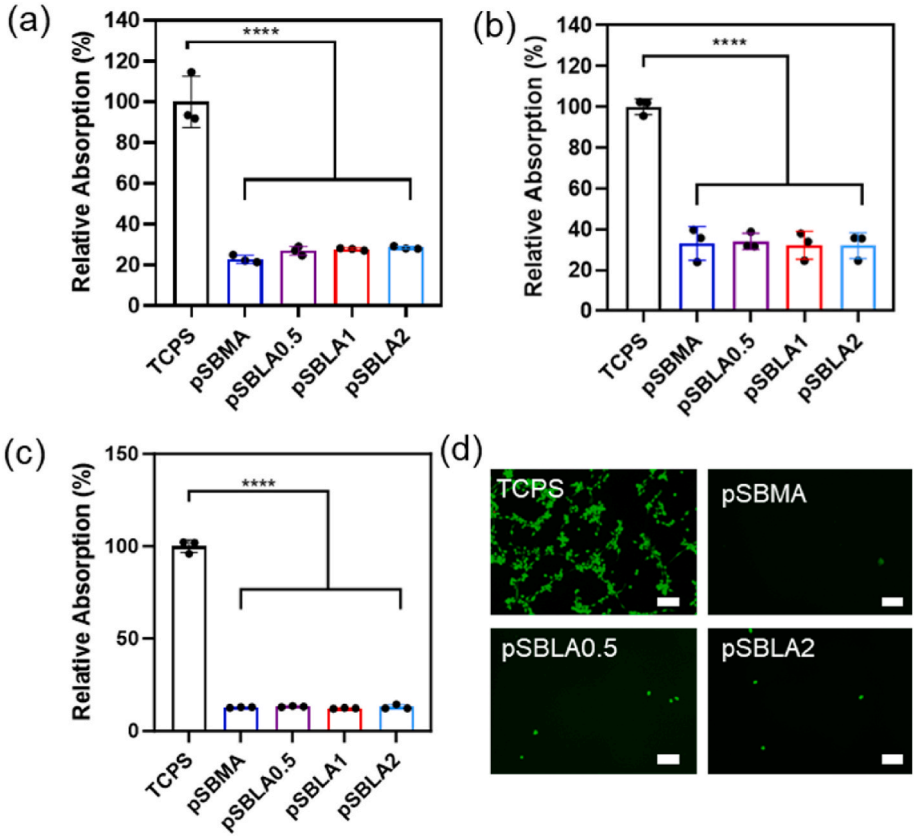

Fig. 3. The nonfouling performances of pSBLA hydrogels *in vitro*. The relative adhesion behaviors of the (a) fibrinogen, (b) BSA, and (c) platelets on tissue culture polystyrene (TCPS) and different hydrogel. (n = 3, ****p < 0.0001). (d) Fluorescent images a of NIH/3T3 cells cultured for 24 h on different hydrogel surfaces. Scar bar = 100 μm.

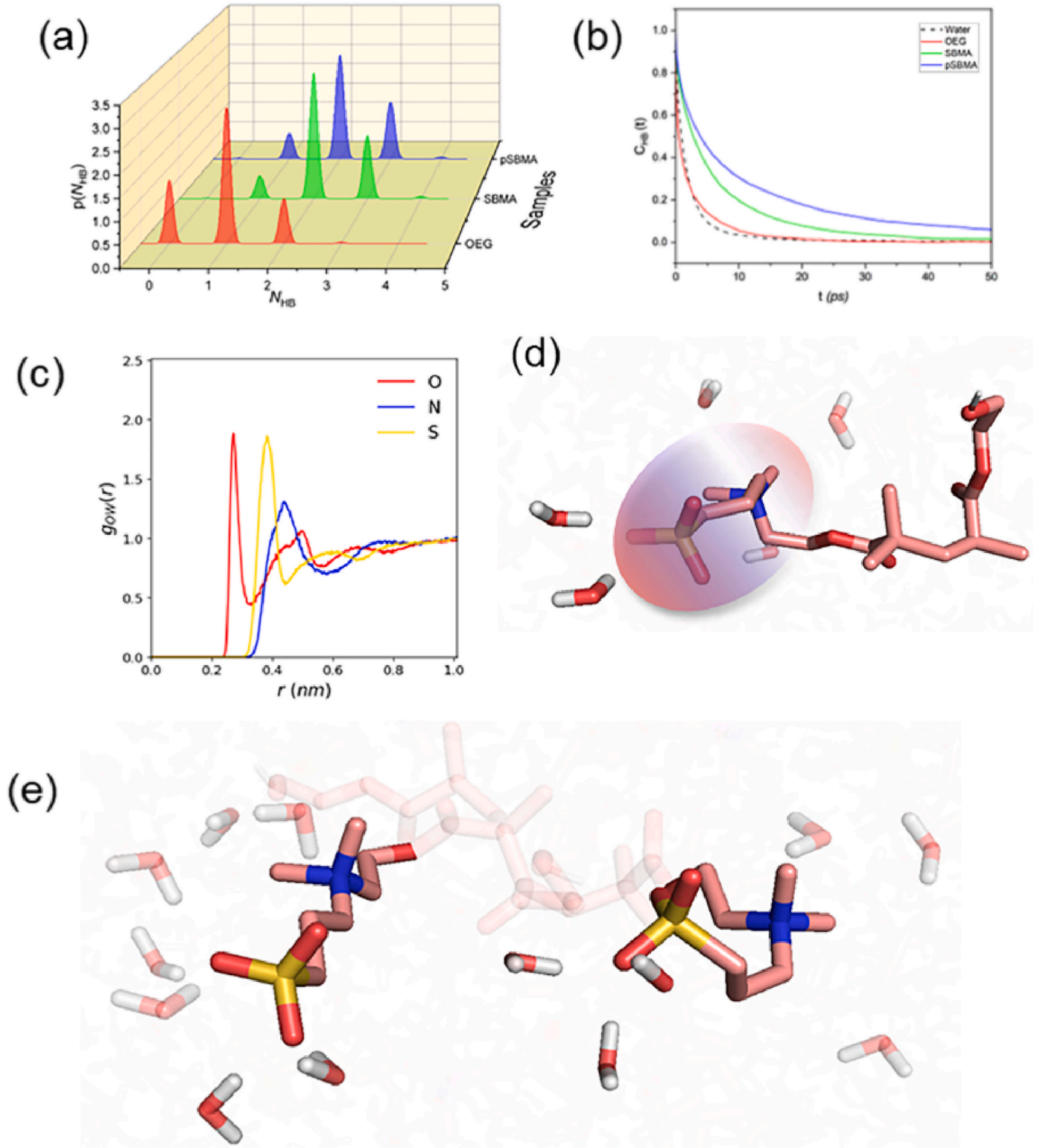

Fig. 4. The mechanism of the protein and cell resistance was investigated at molecular level by MD simulation. (a) The probability distributions for the number of hydrogen bonds. (b) Autocorrelation function for τ_{HB}, C_{HB} (t), for water-SBMA sulfonyl oxygen, water-pSBMA sulfonyl oxygen, water-OEG hydroxyl oxygen, and water-water hydrogen bonds. (c) RDF of water oxygen with respect to one sulfonyl O, N, and S atoms of SBMA. (d) Snapshot of aqueous SBMA with opaque water corresponding to the main peak in the RDF of water oxygen with respect to O (high opacity), N, S atoms of SBMA, respectively. (e) Snapshot of pSBMA in aqueous solution, highlighting the tightly bound waters near two of the SBMA headgroup.

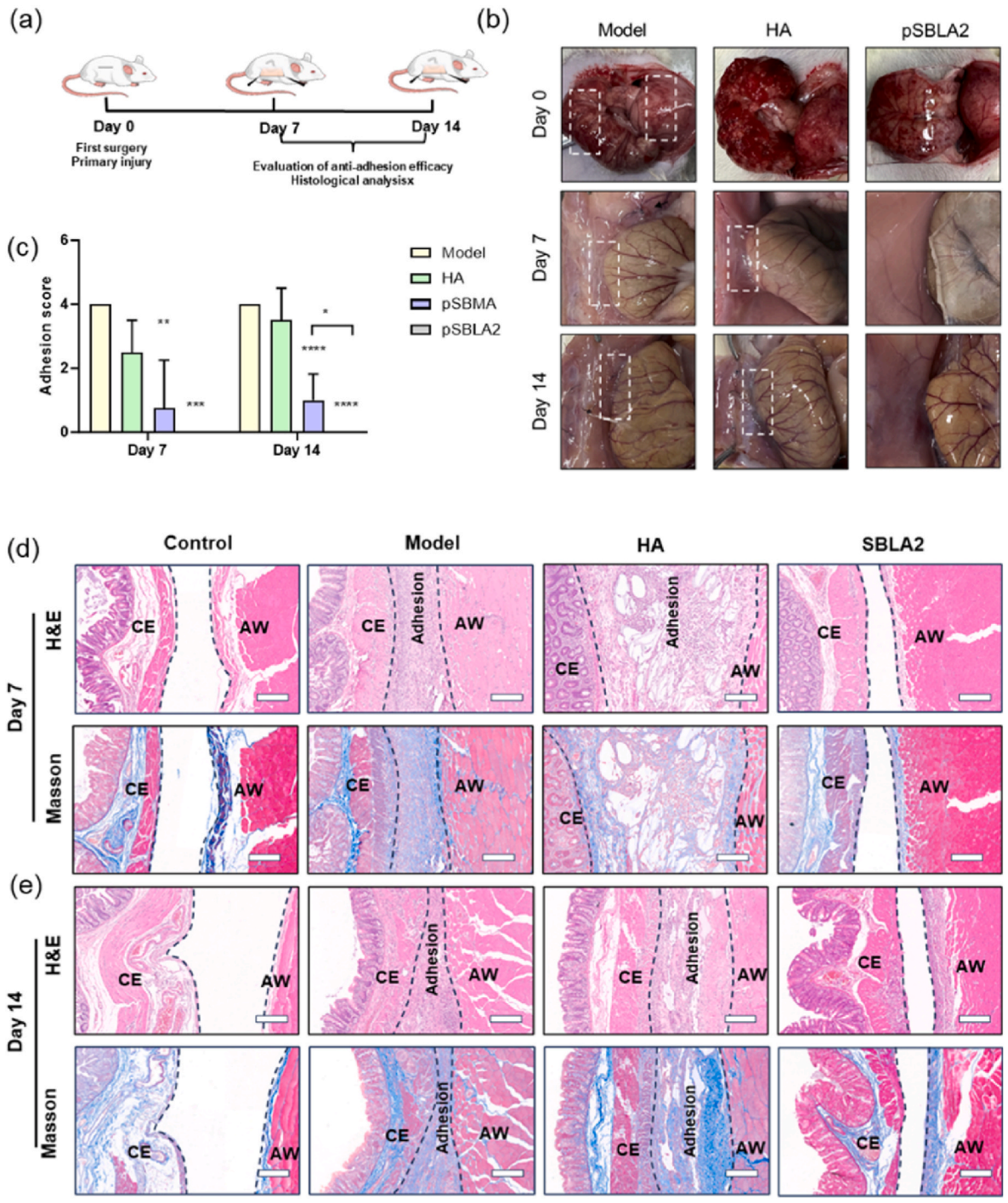

Fig. 5. Evaluation of the pSBLA hydrogel for preventing postsurgical abdominal adhesion using a rat sidewall defect-cecum abrasion adhesion model. (a) Schematic of the procedure schedule. (b) Photographs of peritoneal adhesions in the model, HA hydrogel, and pSBLA2 hydrogel group on postoperative day 7 and 14. (c) Adhesion score of the different degrees in each group on the predetermined time points. (n = 4, ****p < 0.0001). Representative H&E and Masson trichrome staining of adhesive tissues from different groups on day 7 (d) and day 14 (e) after first surgery. CE: cecal mucosa; AW: abdominal wall, Scale bar = 200 μm.

groups was assessed using a standard adhesion scoring system [45]. As shown in Fig. 5b, the absence of a barrier resulted in PA in all rats in the model group, with scores of 4 on the 7th day. HA treatment showed limited efficacy in preventing adhesions, with 3 out of 4 rats scoring 2. However, rats treated with the pSBLA2 hydrogel exhibited no PA formation (model: 4, HA:2.5, pSBLA2: 0). Fourteen days post-operation, rats in the HA groups exhibited heavy adhesions, as indicated by high average scores (model: 4 and HA: 3.5), whereas treatment with the pSBLA2 hydrogel effectively prevented adhesion with an average score of 0 (Fig. 5c). Notably, the surface of the wounds treated with pSBLA2 hydrogel in the above animal experiments was smooth, indicating that the injury had completely healed.

Furthermore, histological examination of the corresponding traumatized tissue on days 7 and 14 was performed using hematoxylin-eosin (H&E) and Masson's trichrome staining to investigate the effects of the pSBLA2 hydrogel (Fig. 5d and e). On day 7, model group showed severe and persistent adhesion, which could not be removed, however, the adhesion layer was relatively loose in the HA group, indicating the anti-

adhesion effect of HA hydrogel. Several inflammatory cells were seen around the traumatized tissue with H&E staining, indicating that the inflammatory response promoted adhesions. In contrast, histological analyses of surgical sites with H&E staining showed that the abdominal sidewall and cecum were separated in the pSBLA2 hydrogel, and some inflammatory cells were observed in the mesothelial layer on day 7; however, no significant inflammatory cells were observed at day 14, suggesting that the damaged tissue was in the recovery stage [46]. In the model group, the adhesion tissue between the abdominal sidewall and cecum became denser by14th day compared to on the 7th day. Besides, HA does not completely cure peritoneal adhesions. In rats treated with the pSBLA2 hydrogel, adhesion formation was absent, and a noticeable reduction in inflammation at the wound site indicated normal tissue recovery. Masson's trichrome staining showed substantial deposition of collagen fibers in the damaged areas of the peritoneum and the sites of adhesion in the model group, attributable to fibroblast proliferation. The HA hydrogel group showed a small amount of collagen fiber deposition in the adhesion layer whereas the pSBLA2 hydrogel group did not show obvious fusion of connective tissue or collagen fiber deposition [27]. These findings indicated that the pSBLA2 hydrogel had a significant preventive effect on abdominal adhesions. Importantly, we thought that those ability of anti-adhesion attributed to the structure of zwitterions. Therefore, we speculated that pSBMA hydrogels also have excellent anti-adhesion ability in vivo. To validate the efficacy of pSBMA hydrogel

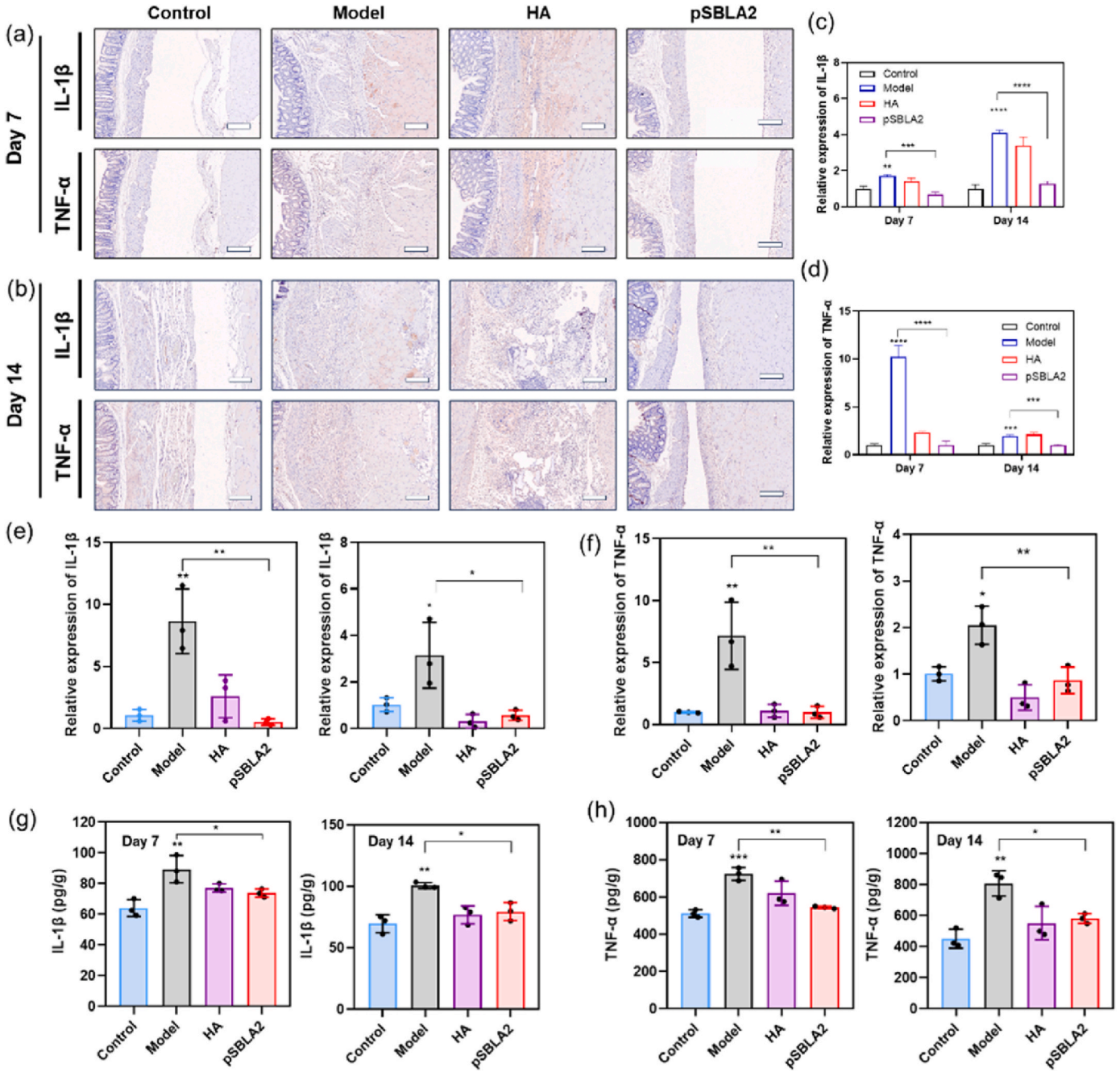

Fig. 6. Expression levels of TNF-α and IL-1β in injured tissues of different groups. (a, b) Immumohistochemical staining of injured tissues after 7 day and 14 day (scale bar = 200 μm). Quantitative analyses of (c) IL-1β and (d) TNF-α (n = 3, *p < 0.05, ***p < 0.001, ****p < 0.0001). The mRNA levels of (e) IL-1β and (f) TNF-α in injured tissues from different groups. (g, h) Effect of pSBLA2 hydrogel on the expression of cytokine IL-1β and TNF-α in tissue on day 7,14 post-operation (n = 3, *p < 0.05, **p < 0.01, ****p < 0.0001, compared with control group).

in preventing PA, we established a sidewall defect-cecum abrasion model of rats. The pSBMA hydrogel also have a significant preventive effect on abdominal adhesions as shown in Fig. S9a. Fourteen days post-operation, rats in the pSBMA groups exhibited slight adhesions with an average score of 1.25 (Fig. 5c), which was significantly different from that of the pSBLA2 group. This may be because the pSBLA2 hydrogel can keep its structure and morphology for 14 days (Fig. S9b).

3.7. Tissue adhesion in vitro

We also found that the pSBLA2 hydrogel could attached to all major organs (heart, liver, spleen, lungs, and kidneys) and different materials (metal, wood, glass, and plastic) (Fig. S10a and b). Furthermore, the hydrogel was capable of conforming to the irregular surfaces of the cecum and liver, demonstrating sufficient adhesion over extended periods without detachment (Fig. S10c, supporting information).

The bonding strength to tissues surrounding the wound was one of the major concerns of materials. Herein, shear adhesion tests of the hydrogels were performed using the test setup shown in Fig. S11a. The average adhesive strength of pSBLA2 hydrogels was 67.5 ± 5.4 kPa, which was significantly higher than those of pSBMA, pSBLA0.5 and pSBLA1 hydrogels (21.6 ± 0.86, 42.0 ± 4.8, and 47.5 ± 2.5 kPa, respectively; Fig. S11a and b). The pSBLA2 hydrogels remained intact and tightly adhered to the porcine skin without detachment after stretching, twisting, or water immersion (Fig. S11c, supporting information). These results indicated that the pSBLA2 hydrogel had considerable tissue-binding strength.

3.8. Underlying mechanism

The mechanism of PA formation is complex and involves many cytokines, cell proliferation and transformation, and signaling pathways [47]. When the abdominal wall and cecum are damaged, the injured peritoneal mesothelial cells produce inflammation-related immune responses, such as increases in the levels of interleukin-1β (IL-1β) and tumor necrosis factor-α (TNF-α) [48,49]. Immunochemical staining of IL-1β and TNF-α was performed to estimate the inflammatory reaction of wounds. The results indicated that IL-1β and TNF-α expression was significantly higher in the model and HA groups than in the pSBLA2 group on days 7 and 14 (Fig. 6a–d). Similarly, on days 7 and 14, the

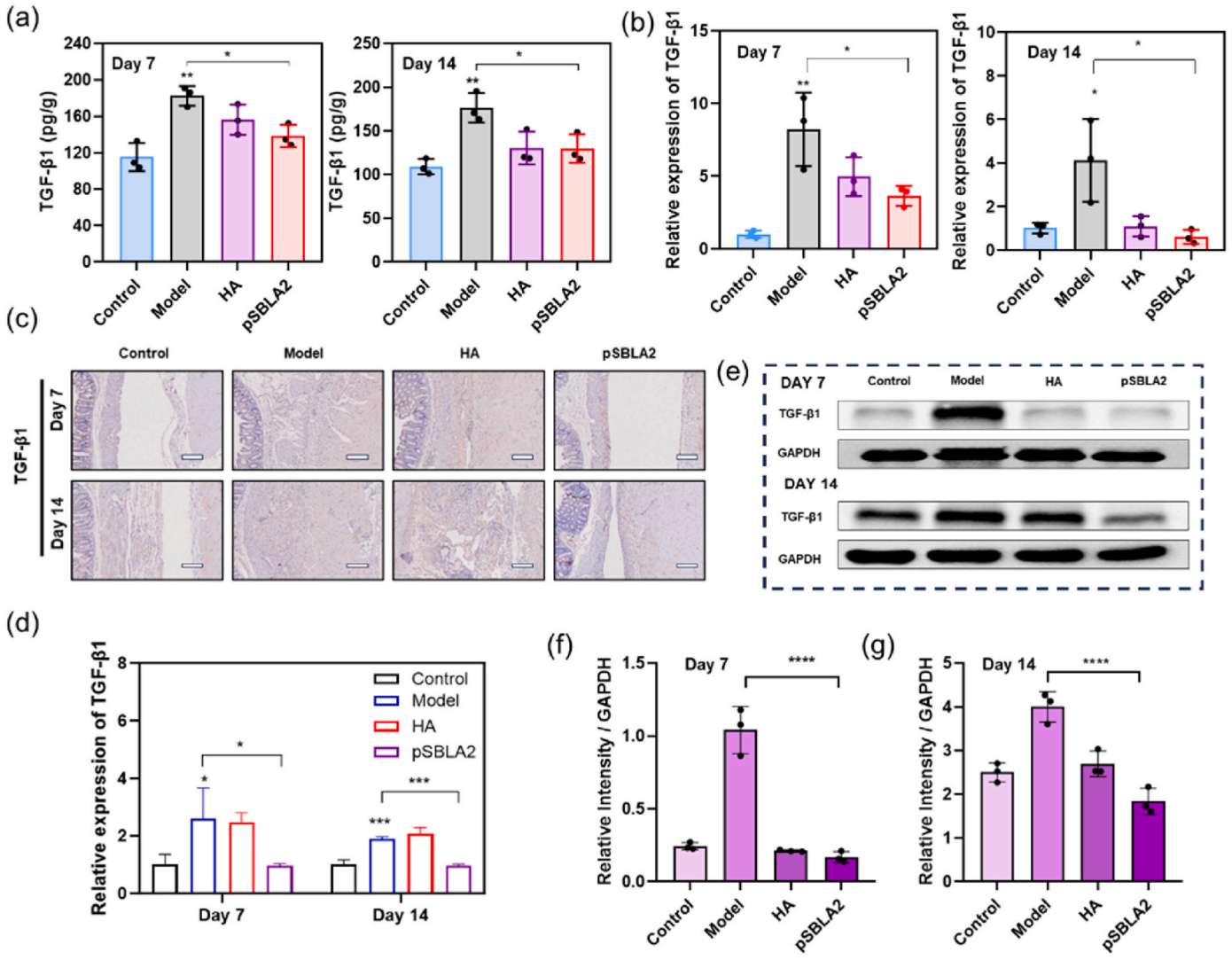

Fig. 7. Expression levels of TGF-β1 in injured tissues of different groups. (a) Secretion levels of TGF-β1 from tissues after treatment with different materials on day 7 and day14 by ELISA (n = 3, *p < 0.05, **p < 0.01, ****p < 0.0001). (b) mRNA levels of representative TGF-β1 in tissues after different treatment (n = 3, *p < 0.05, **p < 0.01, ****p < 0.0001). (c) Immumohistochemical staining and (d) quantitative analyses of injured tissues after 7 day and 14 days (scale bar = 200 μm, n = 3, *p < 0.05, **p < 0.01, ***p < 0.001, ****p < 0.0001). (e) Expression levels and (f, g) quantitative analyses of TGF-β1 markers in tissue via WB assay on day 7,14 post-operation.

tissues treated with pSBLA2 hydrogel showed significantly lower mRNA levels of major pro-inflammatory cytokines, including TNF-α and IL-1β, compared to the model and HA groups. Moreover, treatment with the pSBLA2 hydrogel significantly prevented the increase in mRNA levels of TNF-α and IL-1β, resulting in expression levels similar to that control group, suggesting that the wound completely healed (Fig. 6e-f).

We further monitored the pro-inflammatory response by measuring the secretion of inflammation-related cytokines. ELISA revealed that the levels of TNF-α and IL-1β significantly increased in the model group. However, this trend was reversed following treatment with HA or the pSBLA2 hydrogel (Fig. 6g and h). IL-1β and TNF-α levels in the pSBLA2 hydrogel group were not significantly different from those of control group. These results suggested that the pSBLA2 hydrogel could significantly reduce the levels of inflammatory cytokines after surgical trauma.

TGF-β1 is a key fibrosis factor in these fibrotic processes, and inhibiting its expression can efficiently regulate fibroblasts and the adhesion process [20,50]. Consequently, the expression of TGF- β1was determined. The ELISA conducted on the extracted tissues revealed a significant increase in TGF-β1 secretion in the model group (Fig. 7a). However, this trend was reversed following inoculation on the pSBLA2 hydrogel, in which the TGF-β1 expression was significantly decreased compared to that in the model group. Additionally, the mRNA levels were monitored through q-PCR (Fig. 7b), indicating a highly consistent trend. The immunochemical staining and quantified data (Fig. 7c and d) also revealed that TGF-β1 expression was notably lower on days 7 and 14 in wounds treated by pSBLA2 than in those treated with HA. Moreover, the production of TGF-β1 in tissues was measured by western blotting that showed that the pSBLA2 group induced the lowest expressions of TGF-β1 among all treatments (Fig. 7e and f). Therefore, the pSBLA2 hydrogel could significantly downregulate TGF-β1 expression, indicating that the hydrogel had a potential regulatory effect on peritoneal fibrosis.

TGF-β1 promotes extracellular matrix synthesis via activation of the TGF-β/Smad signaling pathway, ultimately leading to tissue fibrosis [12]. Specifically, elevated TGF-β1 levels can activate downstream Smad2/3, resulting in pro-fibrotic cytokine production such as plasminogen activator inhibitor-1, which exacerbates peritoneal fibrosis [20,50]. In contrast, Smad7 inhibits TGF-β1 signaling by competitively binding to TGF-β1 receptor I (RI) or inducing its degradation [51]. Therefore, the levels of Smad 2/3 and Smad7 were evaluated through immunofluorescence staining (Fig. 8a–d). The expression of Smad2/3 was significantly higher in the model group on days 7 and 14 (green fluorescence intensity) than in the pSBLA2 and HA groups; however, the pSBLA2 hydrogel and control groups did not differ significantly. Notably, Smad7 expression in the pSBLA2 hydrogel group was significantly increased (green fluorescence intensity).

Western blotting analysis showed that the model group had significantly increased Smad2/3 protein expression compared to that of the

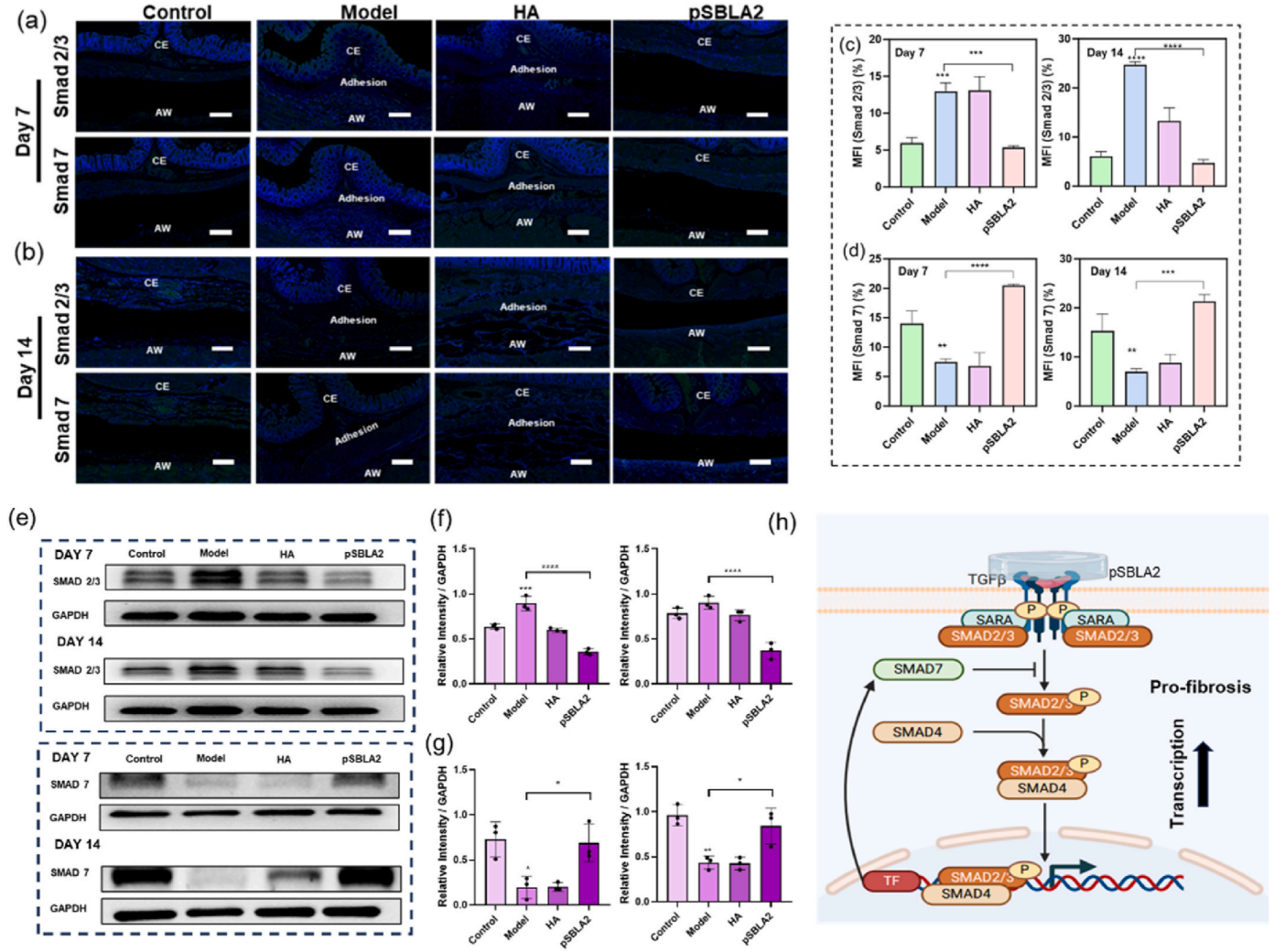

Fig. 8. (a, b) Representative images of immunofluorescence staining of Smad 2/3 and Smad 7 on day 7 and day 14. (c, d) Mean fluorescence intensity (MFI) of Smad2/3 and Smad7 on day 7 and day 14, respectively. (n = 3, ****p < 0.0001). (e–g) Western blot analysis and quantitative of protein expressions (Smad2/3 and Smad7) on day 7, 14. (H) Molecular mechanism of pSBLA2 hydrogel in preventing postoperative abdominal adhesions. (Created with BioRender.com).

control group on days 7 and 14 (Fig. 8e and f). In contrast, the pSBLA2 hydrogel group exhibited significantly decreased Smad2/3 and significantly increased Smad7 expression (Fig. 8f and g). Accordingly, we determined that pSBLA2 hydrogel significantly suppresses Smad2/3 expression, while markedly enhancing Smad7 expression, thereby effectively intervening in the process of peritoneal fibrosis (Fig. 8h). Based on the above result, the pSBLA hydrogel can activate the Smad7 signaling and inhibit the Smad2/3 signaling pathway, there by suppressing inflammation. There mechanisms work together to effectively prevent recurrent adhesion.

3.9. *In vivo biosafety*

In addition, H&E staining showed small aggregation of inflammatory cells at the tissue interface, indicating mild inflammation (Fig. S12, supporting information). Notably, no remarkable pathological abnormalities were noticed in the sections of the major organs (the heart, liver, spleen, lungs and kidneys) (Fig. S13, Supporting Information), indicating that the pSBLA2 hydrogel exhibited excellent biocompatibility. Since the pSBLA2 hydrogel is not toxic to the tissue, it can be integrally removed from the tissue following testing.

3.10. *Prevention of recurrent adhesions by the pSBLA hydrogel*

Blunt dissection is a commonly used method for treating adhesions in clinical practice. However, this may lead to secondary tissue damage, which can promote the formation of more severe adhesions, which are more complex and harder to treatment than primary adhesions [52]. Herein, we established a recurrent adhesion model to evaluate the potential of pSBLA2 hydrogel on recurrent adhesions (Fig. 9a).

On the 7th day of the recurrent adhesion model, the abdominal cavity of rats was opened to assess the effect of hydrogels on preventing adhesion (Fig. 9b). As expected, all rats in the model group showed severe tissue adhesions with a score of 4. In contrast, the average score of the pSBLA2 hydrogel group was 1, which was lower than those of the HA hydrogel (score: 3.5) and model (score: 4) (Fig. 9d). The weight change curve indicated that the model was successfully established (Fig. 9c). H&E and Masson's trichrome staining revealed extensive adhesions in the model group, with a large number of inflammatory cells surrounding the lesions and dense collagen fiber deposition (Fig. 9e and f). However, there is no significant adhesions between the abdominal wall and cecum in the pSBLA2 group. This indicated that the pSBLA2 hydrogel demonstrates promising prospects in the secondary damage caused by adhesiolysis.

The therapeutic mechanism of pSBLA2 hydrogel on recurrent adhesions was further validated. The same relative trend was observed both of TNF-α and IL-1β in the sequence of pSBLA2 hydrogel < HA hydrogel < model group (Figs. S14 and S15, Supporting Information). These results suggested that the pSBLA2 hydrogel significantly inhibited inflammatory reactions after surgical trauma, which effectively prevented secondary adhesions after adhesiolysis. Additionally, ELISA revealed that the levels of TGF-β1 is much lower in wounds treated by

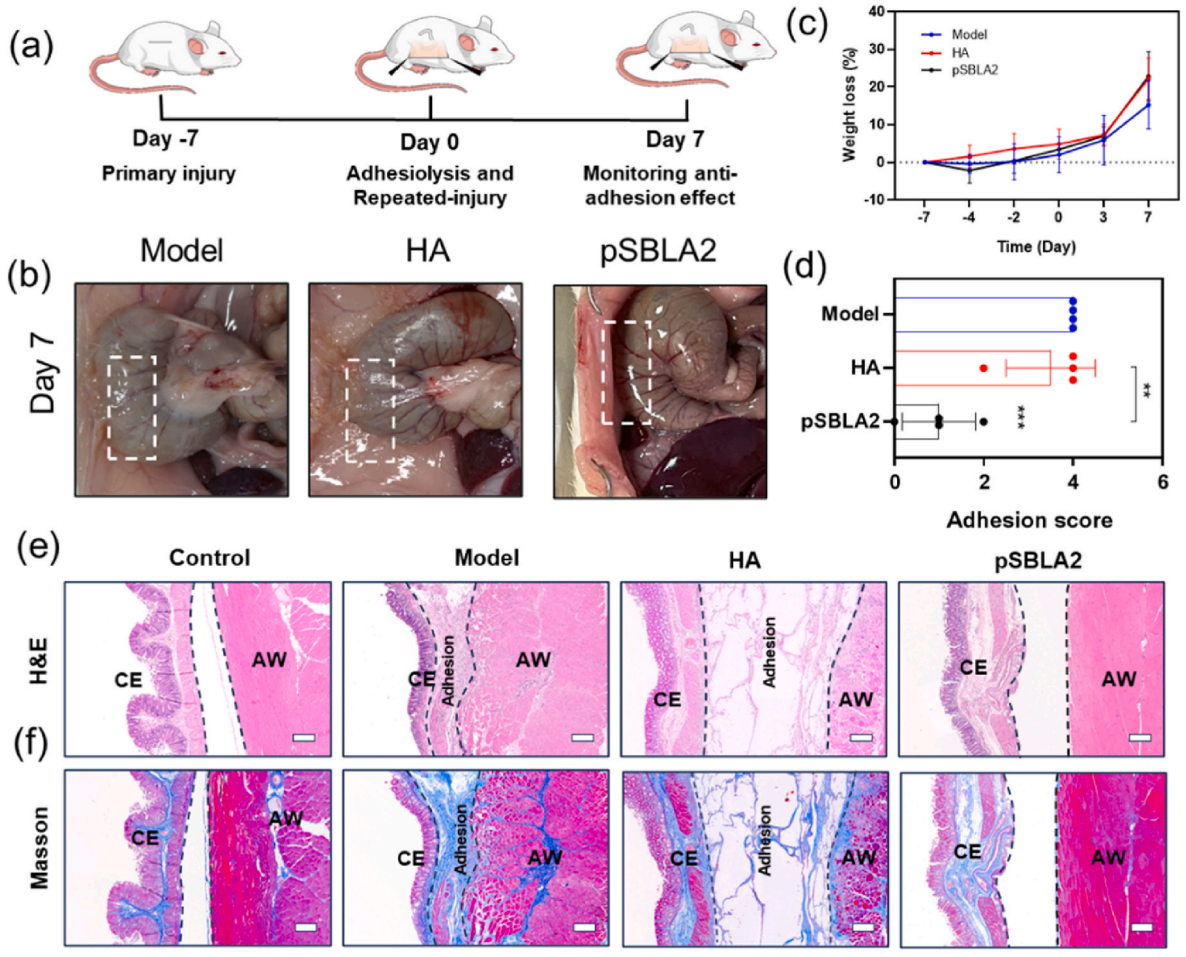

Fig. 9. Evaluation of the pSBLA hydrogel for preventing postsurgical recurrent adhesion using a rat sidewall defect-cecum abrasion adhesion model. (a) Schematic of the procedure schedule. (b) Photographs of peritoneal adhesions in the model, HA hydrogel, and pSBLA2 hydrogel group on day 7 after adhesiolysis. (c) The relative body weight and (d) adhesion score of the different degrees in each group on day 7 after adhesiolysis. (n = 4, ***p < 0.001, ****p < 0.0001). (e, f) H&E and Masson trichrome staining of adhesive tissues from different groups on day 7 after adhesiolysis. Scale bars = 200 μm. CE: cecal mucosa; AW: abdominal wall.

pSBLA2 on day 7 after adhesiolysis, in comparison with the model group (Fig. S16, Supporting Information). We speculate that pSBLA2 hydrogel can also intervene the process of recurrent adhesions by the TGF-β-Smad2/3 signal pathway, but more research is needed. Therefore, we believe that pSBLA hydrogel has great potential in clinic practice as a physical barrier that can rapidly prevent postoperative adhesion and recurrent adhesion.

4. Conclusion

In summary, we designed and prepared, pSBLA, a novel zwitterionic nanocomposite hydrogel using laponite and monomer in a one-pot UV-curable method, to prevent peritoneal PAs. The embedding of nano-silicates in hydrogels was confirmed by the mass loss by TGA, and the presence of Mg and Si atoms by EDS, XPS, and FT-IR. The unique microstructure of laponites, such as charge distribution and hydrogen bonding resulted in good mechanical properties, proliferation and biocompatibility. The pSBLA hydrogel possessed excellent resistance to proteins, and cell adhesion, due to the superhydrophilicity and anti-fouling characteristics of zwitterionic polymers. Besides, we found that pSBLA hydrogel facilitated the proliferation of fibroblast. Additionally, at the molecular level, we used MD simulations to show that the robust antifouling capabilities of pSBLA hydrogels mainly originates from the zwitterionic SBMA segments. Remarkably, in vivo experiments involving cecum-sidewall model and recurrent adhesions illustrate the pSBLA2 hydrogel superior anti-adhesion effectiveness compared to commercial controls. The pSBLA hydrogel act as a physical barrier to prevent adhesion and was able to inhibit inflammatory responses and regulate the TGF-β/Smad signaling pathway to ultimately resist fibrosis. We expect the pSBLA hydrogel to be a next generation anti-adhesion material that addresses safety, efficacy, and operational convenience to meet current clinical needs.

CRediT authorship contribution statement

Weihan Zhu: Writing – original draft, Validation, Methodology, Formal analysis, Data curation, Conceptualization. **Jintao Fang:** Writing – original draft, Validation, Methodology, Formal analysis, Conceptualization. **Wenjun Xu:** Writing – original draft, Visualization, Methodology, Formal analysis, Conceptualization. **Dian Yu:** Methodology, Formal analysis, Conceptualization. **Jintao Shi:** Methodology, Formal analysis, Conceptualization. **Qing Xia:** Writing – review & editing, Resources, Project administration, Funding acquisition, Data curation. **Jinwei Wang:** Investigation, Formal analysis, Conceptualization. **Xiaohui Chen:** Methodology, Formal analysis, Conceptualization. **Haorui Zha:** Methodology, Formal analysis, Conceptualization. **Shengyu Li:** Writing – review & editing, Resources, Project administration, Funding acquisition, Data curation. **Wei Zhang:** Writing – review & editing, Resources, Project administration, Funding acquisition, Data curation.

Declaration of competing interest

The authors declare that they have no known competing financial interests or personal relationships that could have appeared to influence the work reported in this paper.

Acknowledgments

We are grateful for the financial support from the Natural Science Foundation of Zhejiang Province (LQ24H150001), National Natural Science Foundation of China (82304728, 82274475), Medical Health Science and Technology project of Zhejiang Province (2024KY730, 2025KY566). We also appreciate the great help/technical support/experimental support from the Medical Research Center, Academy of Chinese Medical Sciences, Zhejiang Chinese Medical University.

Appendix A. Supplementary data

Supplementary data to this article can be found online at https://doi.org/10.1016/j.mtbio.2025.101811.

Data availability

Data will be made available on request.

References

[1] D.S. Foster, C.D. Marshall, G.S. Gulati, M.S. Chinta, A. Nguyen, A. Salhotra, R. E. Jones, A. Burcham, T. Lerbs, L. Cui, M.E. King, A.L. Titan, R.C. Ransom, A. Manjunath, M.S. Hu, C.P. Blackshear, S. Mascharak, A.L. Moore, J.A. Norton, C. J. Kin, A.A. Shelton, M. Januszyk, G.C. Gurtner, G. Wernig, M.T. Longaker, Elucidating the fundamental fibrotic processes driving abdominal adhesion formation, Nat. Commun. 1 (2020) 4061.

[2] P. Krielen, M.W.J. Stommel, P. Pargmae, N.D. Bouvy, E.A. Bakkum, H. Ellis, M. C. Parker, E.A. Griffiths, H. van Goor, R.P.G. Ten Broek, Adhesion-related readmissions after open and laparoscopic surgery: a retrospective cohort study (SCAR update), Lancet 10217 (2020) 33.

[3] X. Liu, X. Qiu, L. Nie, B. Zhou, P. Bu, Y. Li, X. Xue, B. Tang, Q. Feng, K. Cai, Nonswellable hydrogel patch with tissue-mimetic mechanical characteristics remodeling in vivo microenvironment for effective adhesion prevention, ACS Nano 27 (2024) 17651.

[4] R.M. Leclercq, K.W. Van Barneveld, M.H. Schreinemacher, R. Assies, M. Twellaar, N.D. Bouvy, J.W. Muris, Postoperative abdominal adhesions and bowel obstruction. A survey among Dutch general practitioners, Eur. J. Gen. Pract. 3 (2015) 176.

[5] M. Iwase, H. Watanabe, G. Kondo, M. Ohashi, M. Nagumo, Enhanced susceptibility of oral squamous cell carcinoma cell lines to FAS-mediated apoptosis by cisplatin and 5-fluorouracil, Int. J. Cancer 4 (2003) 619.

[6] Z. Liu, J. Liu, Y. Bai, S. Wu, J. Zhao, L. Ren, A bio-inspired janus patch for treating abdominal wall defects, Adv. Funct. Mater. (2024) 2315827.

[7] L. Tian, T. Sun, M. Fan, H. Lu, C. Sun, Novel silk protein/hyaluronic acid hydrogel loaded with azithromycin as an immunomodulatory barrier to prevent postoperative adhesions, Int. J. Biol. Macromol. (2023) 123811.

[8] L. Li, N. Wang, X. Jin, R. Deng, S. Nie, L. Sun, Q. Wu, Y. Wei, C. Gong, Biodegradable and injectable in situ cross-linking chitosan-hyaluronic acid based hydrogels for postoperative adhesion prevention, Biomaterials 12 (2014) 3903.

[9] L.M. Stapleton, A.N. Steele, H. Wang, H. Lopez Hernandez, A.C. Yu, M.J. Paulsen, A.A.A. Smith, G.A. Roth, A.D. Thakore, H.J. Lucian, K.P. Totherow, S.W. Baker, Y. Tada, J.M. Farry, A. Eskandari, C.E. Hironaka, K.J. Jaatinen, K.M. Williams, H. Bergamasco, C. Marschel, B. Chadwick, F. Grady, M. Ma, E.A. Appel, Y.J. Woo, Use of a supramolecular polymeric hydrogel as an effective post-operative pericardial adhesion barrier, Nat. Biomed. Eng. 8 (2019) 611.

[10] H.-M. Chan, N. Erathodiyil, H. Wu, H. Lu, Y. Zheng, J.Y. Ying, Calcium cross-linked zwitterionic hydrogels as antifouling materials, Mater. Today Commun. (2020) 100950.

[11] Q. Guo, H. Sun, X. Wu, Z. Yan, C. Tang, Z. Qin, M. Yao, P. Che, F. Yao, J. Li, In situ clickable purely zwitterionic hydrogel for peritoneal adhesion prevention, Chem. Mater. 15 (2020) 6347.

[12] S. Huang, Y. Fang, B. Yang, P. Kaur, Y. Wang, J. Zhang, Q. Hu, X. Yang, Y. Zhang, G. Zhai, L. Ye, Zwitterionic biodegradable physical hydrogel based on ATRP technology for effective prevention of postoperative tissue adhesion, Mater. Des. (2023) 111727.

[13] E. Roeven, A.R. Kuzmyn, L. Scheres, J. Baggerman, M.M.J. Smulders, H. Zuilhof, PLL-Poly(HPMA) bottlebrush-based antifouling coatings: three grafting routes, Langmuir 34 (2020) 10187.

[14] Y. Zheng, J. Yang, J. Liang, X. Xu, W. Cui, L. Deng, H. Zhang, Bioinspired hyaluronic acid/phosphorylcholine polymer with enhanced lubrication and anti-inflammation, Biomacromolecules 11 (2019) 4135.

[15] F. Surman, M. Asadikorayem, P. Weber, D. Weber, M. Zenobi-Wong, Ionically annealed zwitterionic microgels for bioprinting of cartilaginous constructs, Biofabrication 2 (2024).

[16] F. Ji, W. Lin, Z. Wang, L. Wang, J. Zhang, G. Ma, S. Chen, Development of nonstick and drug-loaded wound dressing based on the hydrolytic hydrophobic poly (carboxybetaine) ester analogue, Acs Appl Mater Inter 21 (2013) 10489.

[17] X.-W. Wang, J. Wang, Y. Yu, L. Yu, Y.-x. Wang, K.-f. Ren, J. Ji, A polyzwitterion-based antifouling and flexible bilayer hydrogel coating, Composites, Part B (2022) 110164.

[18] P. Sarker, T. Lu, D. Liu, G. Wu, H. Chen, M.S. Jahan Sajib, S. Jiang, Z. Chen, T. Wei, Hydration behaviors of nonfouling zwitterionic materials, Chem. Sci. 27 (2023) 7500.

[19] H.-T. Lin, A. Venault, Y. Chang, Zwitterionized chitosan based soft membranes for diabetic wound healing, J. Membr. Sci. (2019) 117319.

[20] J. Gao, J. Wen, D. Hu, K. Liu, Y. Zhang, X. Zhao, K. Wang, Bottlebrush inspired injectable hydrogel for rapid prevention of postoperative and recurrent adhesion, Bioact. Mater. 27 (2022).

[21] B. Li, P. Jain, J. Ma, J.K. Smith, Z. Yuan, H.C. Hung, Y. He, X. Lin, K. Wu, J. Pfaendtner, S. Jiang, Trimethylamine N-oxide-derived zwitterionic polymers: a new class of ultralow fouling bioinspired materials, Sci. Adv. 6 (2019) eaaw9562.

[22] E. Zhang, J. Yang, K. Wang, B. Song, H. Zhu, X. Han, Y. Shi, C. Yang, Z. Zeng, Z. Cao, Biodegradable zwitterionic cream gel for effective prevention of postoperative adhesion, Adv. Funct. Mater. 10 (2021).
[23] E. Zhang, B. Song, Y. Shi, H. Zhu, X. Han, H. Du, C. Yang, Z. Cao, Fouling-resistant zwitterionic polymers for complete prevention of postoperative adhesion, Proc. Natl. Acad. Sci. U. S. A. 50 (2020) 32046.
[24] Q. Yu, H. Sun, L. Zhang, L. Jiang, L. Liang, C. Yu, X. Dong, B. Guo, Y. Qiu, J. Li, H. Zhang, F. Yao, D. Zhu, J. Li, A zwitterionic hydrogel with anti-oxidative and anti-inflammatory properties for the prevention of peritoneal adhesion by inhibiting mesothelial-mesenchymal transition, Adv. Healthc. Mater. 30 (2023) e2301696.
[25] Z. Zhao, H. Sun, C. Yu, B. Liu, R. Liu, Q. Yang, B. Guo, X. Li, M. Yao, F. Yao, H. Zhang, J. Li, Injectable asymmetric adhesive-antifouling bifunctional hydrogel for peritoneal adhesion prevention, Adv. Healthc. Mater. 10 (2024) e2303574.
[26] A. Schmidt, D. Taylor, Erosion of soft tissue by polypropylene mesh products, J. Mech. Behav. Biomed. Mater. (2021) 104281.
[27] J. Yu, K. Wang, C. Fan, X. Zhao, J. Gao, W. Jing, X. Zhang, J. Li, Y. Li, J. Yang, W. Liu, An ultrasoft self-fused supramolecular polymer hydrogel for completely preventing postoperative tissue adhesion, Adv. Mater. 16 (2021) e2008395.
[28] X. Xu, Z. Chen, L. Xiao, Y. Xu, N. Xiao, W. Jin, Y. Chen, Y. Li, K. Luo, Nanosilicate-functionalized nanofibrous membrane facilitated periodontal regeneration potential by harnessing periodontal ligament cell-mediated osteogenesis and immunomodulation, J. Nanobiotechnol. 1 (2023) 223.
[29] J.I. Dawson, J.M. Kanczler, X.B. Yang, G.S. Attard, R.O. Oreffo, Clay gels for the delivery of regenerative microenvironments, Adv. Mater. 29 (2011) 3304.
[30] P. Xu, T. Erdem, E. Eiser, A simple approach to prepare self-assembled, nacre-inspired clay/polymer nanocomposites, Soft Matter 23 (2020) 5497.
[31] W. Yao, Z. Song, X. Ma, Y. Huang, X. Zhang, Y. Li, P. Wei, J. Zhang, C. Xiong, S. Yang, Y. Xu, W. Jing, B. Zhao, X. Zhang, Y. Han, Asymmetric adhesive SIS-based wound dressings for therapeutically targeting wound repair, J. Nanobiotechnol. 1 (2024) 34.
[32] C. Chen, J. Tang, Y. Gu, L. Liu, X. Liu, L. Deng, C. Martins, B. Sarmento, W. Cui, L. Chen, Bioinspired hydrogel electrospun fibers for spinal cord regeneration, Adv. Funct. Mater. 4 (2018).
[33] J. Zhang, L. Chen, L. Chen, S. Qian, X. Mou, J. Feng, Highly antifouling, biocompatible and tough double network hydrogel based on carboxybetaine-type zwitterionic polymer and alginate, Carbohydr. Polym. (2021) 117627.
[34] H. Wang, X. Yi, T. Liu, J. Liu, Q. Wu, Y. Ding, Z. Liu, Q. Wang, An integrally formed janus hydrogel for robust wet-tissue adhesive and anti-postoperative adhesion, Adv. Mater. 23 (2023) e2300394.
[35] Z. Ding, Z. Liang, X. Rong, X. Fu, J. Fan, Y. Lai, Y. Cai, C. Huang, L. Li, G. Tang, Z. Luo, Z. Zhou, Janus-structured microgel barrier with tissue adhesive and hemostatic characteristics for efficient prevention of postoperative adhesion, Small 50 (2024) 2403753.
[36] N. Sallstrom, A. Capel, M.P. Lewis, D.S. Engstrom, S. Martin, 3D-printable zwitterionic nano-composite hydrogel system for biomedical applications, J. Tissue Eng. 11 (2020) 2041731420967294.
[37] A. Al Hossain, M. Yang, A. Checco, G. Doerk, C.E. Colosqui, Large-area nanostructured surfaces with tunable zeta potentials, Appl. Mater. Today (2020) 100593.
[38] M. Manciu, F.S. Manciu, E. Ruckenstein, On the surface tension and Zeta potential of electrolyte solutions, Adv. Colloid Interface Sci. 90 (2017).
[39] Y. Liu, X. Guo, M. Zhao, C. Zou, Y. Feng, Y. Wu, C. Dai, The effect and enhancement mechanism of hydrophobic interaction and electrostatic interaction on zwitterionic wormlike micelles, Colloids Surf., A (2022) 129424.
[40] F. Topuz, A. Nadernezhad, O.S. Caliskan, Y.Z. Menceloglu, B. Koc, Nanosilicate embedded agarose hydrogels with improved bioactivity, Carbohydr. Polym. 105 (2018).
[41] X. Xu, J. Zhuo, L. Xiao, Y. Xu, X. Yang, Y. Li, Z. Du, K. Luo, Nanosilicate-Functionalized polycaprolactone orchestrates osteogenesis and osteoblast-induced multicellular interactions for potential endogenous vascularized bone regeneration, Macromol. Biosci. 2 (2021).
[42] Z. Zhao, M. Pan, C. Qiao, L. Xiang, X. Liu, W. Yang, X.Z. Chen, H. Zeng, Bionic engineered protein coating boosting anti-biofouling in complex biological fluids, Adv. Mater. 6 (2023) e2208824.
[43] Tanji H. Retraction, C. Ishikawa, S. Sawada, S. Nakachi, R. Takamatsu, T. Matsuda, T. Okudaira, J.-N. Uchihara, K. Ohshiro, Y. Tanaka, M. Senba, H. Uezato, K. Ohshima, M. Duc Dodon, K.-J. Wu, N. Mori, Aberrant expression of the transcription factor Twist in adult T-cell leukemia, Blood 8 (2010) 1386, https://doi.org/10.1182/blood-2009-07-232231 [published online ahead of print January 13, 2010].
[44] J. Tang, Z. Xiang, M.T. Bernards, S. Chen, Peritoneal adhesions: occurrence, prevention and experimental models, Acta Biomater. 84 (2020).
[45] Y. Fang, S. Huang, X. Gong, J.A. King, Y. Wang, J. Zhang, X. Yang, Q. Wang, Y. Zhang, G. Zhai, L. Ye, Salt sensitive purely zwitterionic physical hydrogel for prevention of postoperative tissue adhesion, Acta Biomater. 239 (2023).
[46] D. Jin, S. Yang, S. Wu, M. Yin, H. Kuang, A functional PVA aerogel-based membrane obtaining sutureability through modified electrospinning technology and achieving promising anti-adhesion effect after cardiac surgery, Bioact. Mater. 355 (2022).
[47] Y. Bian, L. Yang, B. Zhang, W. Li, S. Wang, S. Jiang, X. Chen, W. Li, L. Zeng, LincRNA cox-2 regulates lipopolysaccharide-induced inflammatory response of human peritoneal mesothelial cells via modulating miR-21/NF-kappaB Axis, Mediat. Inflamm. (2019) 8626703.
[48] X. Ge, H. Wen, Y. Fei, R. Xue, Z. Cheng, Y. Li, K. Cai, L. Li, M. Li, Z. Luo, Structurally dynamic self-healable hydrogel cooperatively inhibits intestinal inflammation and promotes mucosal repair for enhanced ulcerative colitis treatment, Biomaterials (2023) 122184.
[49] S. Qi, R. Luo, X. Han, W. Nie, N. Ye, C. Fu, F. Gao, pH/ROS dual-sensitive natural polysaccharide nanoparticles enhance "one stone four birds" effect of rhein on ulcerative colitis, ACS Appl. Mater. Interfaces 45 (2022) 50692.
[50] P. Patel, Y. Sekiguchi, K.H. Oh, S.E. Patterson, M.R. Kolb, P.J. Margetts, Smad3-dependent and -independent pathways are involved in peritoneal membrane injury, Kidney Int. 4 (2010) 319.
[51] H. Zhang, Y. Song, Z. Li, T. Zhang, L. Zeng, Evaluation of breviscapine on prevention of experimentally induced abdominal adhesions in rats, Am. J. Surg. 6 (2016) 1143.
[52] K. Isaacson, Lysis of mid-uterine central adhesions has lower recurrence risk, BJOG 4 (2016) 624.